

MixedNUTS: Training-Free Accuracy-Robustness Balance via Nonlinearly Mixed Classifiers

Yatong Bai¹ Mo Zhou² Vishal M. Patel² Somayeh Sojoudi¹

Abstract

Adversarial robustness often comes at the cost of degraded accuracy, impeding the real-life application of robust classification models. Training-based solutions for better trade-offs are limited by incompatibilities with already-trained high-performance large models, necessitating the exploration of training-free ensemble approaches. Observing that robust models are more confident in correct predictions than in incorrect ones on clean and adversarial data alike, we speculate amplifying this “benign confidence property” can reconcile accuracy and robustness in an ensemble setting. To achieve so, we propose “MixedNUTS”, a *training-free* method where the output logits of a robust classifier and a standard non-robust classifier are processed by nonlinear transformations with only three parameters, which are optimized through an efficient algorithm. MixedNUTS then converts the transformed logits into probabilities and mixes them as the overall output. On CIFAR-10, CIFAR-100, and ImageNet datasets, experimental results with custom strong adaptive attacks demonstrate MixedNUTS’s vastly improved accuracy and near-SOTA robustness – it boosts CIFAR-100 clean accuracy by 7.86 points, sacrificing merely 0.87 points in robust accuracy.

1. Introduction

Neural classifiers are vulnerable to adversarial attacks, producing unexpected predictions when subject to purposefully constructed human-imperceptible input perturbations and hence manifesting severe safety risks (Goodfellow et al., 2015; Madry et al., 2018). Existing methods for robust deep neural networks (Madry et al., 2018; Zhang et al., 2019) often suffer from significant accuracy penalties on clean (unattacked) data (Tsipras et al., 2019; Zhang et al., 2019; Pang et al., 2022). As deep models continue to form the core of numerous products, trading clean accuracy for robustness is understandably unattractive for real-life users

¹University of California, Berkeley. ²John Hopkins University. Correspondence to: Yatong Bai <yatong_bai@berkeley.edu>. Code available at github.com/Bai-YT/MixedNUTS.

and profit-driven service providers. As a result, despite the continuous development in adversarial robustness research, robust models are rarely deployed and practical services remain non-robust (Ilyas et al., 2018; Borkar & Chen, 2021).

To bridge the gap between robustness research and applications, researchers have considered reconciling robustness and accuracy (Balaji et al., 2019; Chen et al., 2020; Raghunathan et al., 2020; Rade & Moosavi-Dezfooli, 2021; Liu & Zhao, 2022; Pang et al., 2022; Cheng et al., 2022). Most works focused on improving robust training methods, and are thus expensive to implement. Moreover, training-based methods may be incompatible with each other, and can be hard to integrate into recent advancements in large-scale models pre-trained with large real or synthetic datasets. An alternative direction to relieve the accuracy-robustness trade-off is through an ensemble of a standard (often non-robust) model and a robust model Bai et al. (2023b;a). This ensemble model is referred to as the *mixed classifier*, whereas *base classifiers* refers to its standard and robust components.

We observe that many robust base models share a benign confidence property: their correct predictions are much more confident than incorrect ones. Verifying such a property for numerous existing models trained via different methods (Peng et al., 2023; Pang et al., 2022; Wang et al., 2023; Debenedetti et al., 2022; Na, 2020; Gowal et al., 2020; Liu et al., 2023; Singh et al., 2023), we speculate that strengthening this property can improve the mixed classifiers’ trade-off even without changing the base classifiers’ predicted classes.

Based on this intuition, we propose MixedNUTS (Mixed neUral classifiers with Nonlinear TranSformation), a training-free method that enlarges the robust base classifier confidence difference between correct and incorrect predictions and thereby optimizes the mixed classifier’s accuracy-robustness trade-off. MixedNUTS applies nonlinear transformations to the accurate and robust base classifiers’ logits before converting them into probabilities used for mixing. We parameterize the transformation with only three coefficients and design an efficient algorithm to optimize them for the best trade-off. Unlike (Bai et al., 2023a), MixedNUTS does not modify base neural network weights or introduce additional components and is for the first time efficiently extendable to larger datasets such as ImageNet. MixedNUTS is compatible with various pre-trained standard and

robust models and is agnostic to the base model details such as training method, defense norm (ℓ_∞ , ℓ_2 , etc.), training data, and model architecture. Therefore, MixedNUTS can take advantage of recent developments in accurate or robust classifiers while being general, lightweight, and convenient.

Our experiments leverage AutoAttack (Croce & Hein, 2020) and strengthened adaptive attacks (details in Appendix B) to confirm the security of the mixed classifier and demonstrate the balanced accuracy and robustness on datasets including CIFAR-10, CIFAR-100, and ImageNet. On CIFAR-100, MixedNUTS improves the clean accuracy by 7.86 percentage points over the state-of-the-art non-mixing robust model while reducing robust accuracy by merely 0.87 points.

2. Background and Related Work

2.1. Definitions and Notations

This paper uses $\sigma : \mathbb{R}^c \rightarrow (0, 1)^c$ to denote the standard Softmax function: for an arbitrary $z \in \mathbb{R}^c$, the i^{th} entry of $\sigma(z)$ is defined as $\sigma(z)_i := \frac{\exp(z_i)}{\sum_{j=1}^c \exp(z_j)}$, where z_i denotes the i^{th} entry of z . Consider the special case of $z_i = +\infty$ for some i , with all other entries of z being less than $+\infty$. We define $\sigma(z)$ for such a z vector to be the basis (one-hot) vector e_i . For a classifier $h : \mathbb{R}^d \rightarrow \mathbb{R}^c$, we use the composite function $\sigma \circ h : \mathbb{R}^d \rightarrow [0, 1]^c$ to denote its output probabilities and use $\sigma \circ h_i$ to denote the i^{th} entry of it.

We define the notion of *confidence margin* of a classifier as the output probability gap between the top two classes:

Definition 2.1. Consider a model $h : \mathbb{R}^d \rightarrow \mathbb{R}^c$, an arbitrary input $x \in \mathbb{R}^d$, and its associated predicted label $\hat{y} \in [c]$. The *confidence margin* is defined as $m_h(x) := \sigma \circ h_{\hat{y}}(x) - \max_{i \neq \hat{y}} \sigma \circ h_i(x)$.

We consider a classifier to be (ℓ_p -norm) robust at an input $x \in \mathbb{R}^d$ if it assigns the same label to all perturbed inputs $x + \delta$ such that $\|\delta\|_p \leq \epsilon$, where $\epsilon \geq 0$ is the attack radius. We additionally introduce the notion of the worst-case adversarial perturbation in the sense of minimizing the margin:

Definition 2.2. Consider an adversarial attack against the confidence margin $m_h(x)$,

$$\min_{\|\delta\| \leq \epsilon} m_h(x + \delta).$$

We define the optimizer of this problem, $\delta_h^*(x)$, as the *minimum-margin perturbation* of $h(\cdot)$ around x . We further define the optimal objective value, denoted as $\underline{m}_h^*(x)$, as the *minimum margin* of $h(\cdot)$ around x .

When the minimum margin is negative, the adversarial perturbation successfully changes the model prediction as a wrong class. When the minimum margin is positive, the model is robust at x , because perturbations within the radius cannot change the prediction.

2.2. Related Adversarial Attacks and Defenses

While the fast gradient sign method (FGSM) and projected gradient descent (PGD) attacks could attack and evaluate certain models (Madry et al., 2018; Goodfellow et al., 2015), they are insufficient and can fail to attack non-robust models (Carlini & Wagner, 2017; Athalye et al., 2018; Papernot et al., 2017). To this end, stronger adversaries leveraging novel attack objectives, black-box attacks, and expectation over transformation have been proposed (Gowal et al., 2019; Croce & Hein, 2020; Tramèr et al., 2020). Benchmarks based on these strong attacks, such as RobustBench (Croce et al., 2020), ARES-Bench (Liu et al., 2023), and OODRobustBench (Li et al., 2023), aim to unify defense evaluation.

AutoAttack (Croce & Hein, 2020) is a combination of white-box and black-box attacks (Andriushchenko et al., 2020). It is the attack algorithm of RobustBench (Croce et al., 2020), where AutoAttack-evaluated robust models are often agreed to be trustworthy. We select AutoAttack as the main evaluator, with further strengthening tailored to our defense.

Models aiming to be robust against adversarial attacks often incorporate adversarial training (Madry et al., 2018; Bai et al., 2022; 2023c), TRADES (Zhang et al., 2019), or their variations. Later work further enhance the adversarial robustness by synthetic training data (Wang et al., 2023; Sehwag et al., 2022), data augmentation (Gowal et al., 2020; Rebuffi et al., 2021; Gowal et al., 2021), improved training loss functions (Cui et al., 2023), purposeful architectures (Peng et al., 2023), or efficient optimization (Shafahi et al., 2019). Nevertheless, training-based methods suffer from the trade-off between clean and robust accuracy, and cannot leverage already-trained state-of-the-art non-robust models.

2.3. Ensemble and Calibration

Model ensembles, where the outputs of multiple models are combined to produce the overall prediction, have been explored to improve model performance (Ganaie et al., 2022) or estimate model uncertainty (Liu et al., 2019). Ensemble techniques have also been considered to strengthen adversarial robustness (Pang et al., 2019; Adam & Speciel, 2020; Alam et al., 2022; Co et al., 2022). Theoretical certified robustness analyses of ensemble models indicate that the robust margins, gradient diversity, and runner-up class diversity all contribute to ensemble robustness (Petrov et al., 2023; Yang et al., 2022). Unlike these existing works that combine multiple robust models, we focus on mixing a robust model and a high-accuracy (usually non-robust) model.

Model calibration often involves adjusting confidence, which aims to align a model's confidence with its mispredicting probability, usually via temperature scaling (Guo et al., 2017; Yu et al., 2022; Hinton et al., 2015). While adjusting confidence of a single model generally does not change the

prediction, it is not the case in the ensemble setting. Unlike most calibration research focusing on uncertainty, this paper adjusts the confidence for performance.

2.4. Mixing Classifiers for Accuracy-Robust Trade-Off

Consider a classifier $g : \mathbb{R}^d \rightarrow \mathbb{R}^c$, whose predicted logits are g_1, \dots, g_c , where d is the input dimension and c is the number of classes. We assume $g(\cdot)$ to be a standard classifier trained for high clean accuracy (and hence may not manifest adversarial robustness). Similarly, we consider another classifier $h : \mathbb{R}^d \rightarrow \mathbb{R}^c$ and assume it to be robust against adversarial attacks. We use *accurate base classifier* and *robust base classifier* to refer to $g(\cdot)$ and $h(\cdot)$.

Mixing the outputs of a standard classifier and a robust classifier improves the accuracy-robustness trade-off, and it has been shown that mixing the probabilities is more desirable than mixing the logits from theoretical and empirical perspectives (Bai et al., 2023b;a). Here, we denote the proposed mixed model with $f : \mathbb{R}^d \rightarrow \mathbb{R}^c$. Specifically, the i^{th} output logit of the mixed model follows the formulation

$$f_i(x) := \log((1 - \alpha) \cdot \sigma \circ g(x)_i + \alpha \cdot \sigma \circ h(x)_i) \quad (1)$$

for all $i \in [c]$, where $\alpha \in [1/2, 1]$ adjusts the mixing weight. The mixing operation is performed in the probability space, and the natural logarithm maps the mixed probability back to the logit space without changing the predicted class for interchangeability with existing models. If the desired output is the probability $\sigma \circ f(\cdot)$, the logarithm can be omitted.

3. Base Classifier Confidence Modification

We observe that the robust base classifier $h(\cdot)$ often enjoys the benign confidence property of having much more confidence in correct predictions than in mistakes, even when subject to adversarial attack. Section 5.2 verifies this property with multiple model examples, and Appendix C.1 visualizes the confidence margin distribution. As a result, when mixing the output probabilities $\sigma \circ h(\cdot)$ and $\sigma \circ g(\cdot)$ on clean data, where g is expected to be more accurate than h , g can correct h 's mistake because h is unconfident. Meanwhile, when the mixed classifier is under attack and h becomes much more reliable than g , h 's high confidence in correct predictions can overcome g 's misguided outputs. Hence, even when g 's robust accuracy is near zero, the mixed classifier still inherits most of h 's robustness.

Note that this benign confidence property is only observed on robust classifiers. Neural classifiers trained without any robustness considerations often make highly confident mispredictions when subject to adversarial attack (more confident than correctly predicted unperturbed examples).

Bai et al. (2023b;a) have shown that α should be no smaller than $1/2$ for $f(\cdot)$ to have non-trivial robustness.

3.1. Accurate Base Classifier Temperature Scaling

Since the mixed classifier's accuracy-robustness trade-off heavily depends on the base classifiers' confidence properties, modifying their confidence has vast potential. To this end, we consider temperature scaling (Hinton et al., 2015).

We start with analyzing the accurate base classifier $g(\cdot)$. One approach to mitigate $g(\cdot)$'s detrimental property of being more confident when mispredicting under attack than when correctly predicting clean data is to scale up its logits prior to the Softmax operation. Specifically, we construct the temperature scaled model $g^{\text{TS},T}(\cdot)$, whose i^{th} entry is

$$g_i^{\text{TS},T}(x) := g_i(x)/T$$

for all i , where $T \geq 0$ is the temperature constant. To scale up the confidence, T should be less than 1.

To understand this operation, observe that temperature scaling increases $g(\cdot)$'s confidence in correct clean examples and incorrect adversarial examples simultaneously. However, because $g(\cdot)$'s confidence under attack is already close to 1 prior to the scaling, the increase in attacked misprediction confidence is negligible due to the saturation of the Softmax function. Since $g(\cdot)$ becomes more confident on correct examples with the mispredicting confidence almost unchanged, its detrimental confidence property is mitigated.

The extreme selection of T for the temperature scaling operation is 0, in which case the predicted probabilities $\sigma \circ g^{\text{TS},0}(\cdot)$ becomes a one-hot vector corresponding to $g(\cdot)$'s predicted class. In addition to mitigating the detrimental confidence property of $g(\cdot)$, selecting $T = 0$ has the additional benefit of simplifying Section 4's analysis on the robust base model $h(\cdot)$ by allowing for a direct connection between $h(\cdot)$'s confidence and the mixed classifier's correctness. Hence, we select $T = 0$ and use $g^{\text{TS},0}(\cdot)$ as the accurate base classifier for the remaining analyses. Appendix B.2 discusses how our attacks circumvent the nondifferentiability resulting from using $T = 0$. Appendix D.1 verifies that $T = 0$ produces the best empirical effectiveness.

A similar temperature scaling operation can be applied to the robust base classifier $h(\cdot)$. Unlike $g(\cdot)$, $h(\cdot)$'s confidence property is benign. To fully unleash its potential, we generalize the idea of confidence modification beyond temperature scaling to allow nonlinear logit transformations, thereby treating low-confidence and high-confidence examples differently and amplifying $h(\cdot)$'s benign property, leading to further mixed classifier accuracy-robustness balance.

4. MixedNUTS - Nonlinearly Mixed Classifier

4.1. Nonlinear Robust Base Classifier Transformation

We aim to build a nonlinearly mapped classifier $h^M(\cdot) := M(h(\cdot))$, where $M \in \mathcal{M} : \mathbb{R}^c \mapsto \mathbb{R}^c$ is a nonlinear trans-

formation applied to the classifier $h(\cdot)$'s logits, and \mathcal{M} is the set of all possible transformations. The prediction probabilities from this transformed robust base model are then mixed with those from $g^{\text{TS},0}(\cdot)$ to form the mixed classifier $f^M(\cdot)$ following (1). For the optimal accuracy-robustness trade-off, we select an M that maximizes the clean accuracy of $f^M(\cdot)$ while maintaining the desired robust accuracy. Formally, this goal is described as the optimization problem

$$\begin{aligned} \max_{M \in \mathcal{M}, \alpha \in [1/2, 1]} & \mathbb{P}_{(X,Y) \sim \mathcal{D}} [\arg \max_i f_i^M(X) = Y] \quad (2) \\ \text{s. t. } & \mathbb{P}_{(X,Y) \sim \mathcal{D}} [\arg \max_i f_i^M(X + \delta_{f^M}^*(X)) = Y] \geq r_{f^M}, \end{aligned}$$

where \mathcal{D} is the distribution of data-label pairs, r_{f^M} is the desired robust accuracy of $f^M(\cdot)$, and $\delta_{f^M}^*(x)$ is the minimum-margin perturbation of $f^M(\cdot)$ at x . Note that $f_i^M(\cdot)$ implicitly depends on M and α .

The problem (2) depends on the robustness behavior of the mixed classifier, which is expensive to probe. Ideally, the optimization should only need the base classifier properties, which can be evaluated beforehand. To allow such a simplification, we make the following two assumptions.

Assumption 4.1. On unattacked clean data, if $h^M(\cdot)$ makes a correct prediction, then $g(\cdot)$ is also correct.

We make this assumption because the clean accuracy of the accurate base classifier $g^{\text{TS},0}(\cdot)$ should be noticeably higher than that of the robust base model $h^M(\cdot)$ to justify the potential advantage of mixing them together. In practice, the amount of clean data correctly predicted by $h^M(\cdot)$, but not by $g^{\text{TS},0}(\cdot)$, is rare and does not make significant impact.

Assumption 4.2. The transformation $M(\cdot)$ does not change the predicted class due to, *e.g.*, monotonicity. Namely, it holds that $\arg \max_i M(h(x))_i = \arg \max_i h_i(x)$ for all x .

We make this assumption because, while it is mathematically possible to find an M that improves the accuracy of $h(\cdot)$, obtaining it could be as hard as training a new improved robust model. On the other hand, many relatively simple transformations can preserve the predicted class of $h(\cdot)$ while enhancing its benign confidence property, and we will propose Algorithm 1 for finding such a transformation.

These two assumptions allow us to decouple the optimization of $M(\cdot)$ from the accurate base classifier $g(\cdot)$. Specifically, we can solve the following optimization problem as a surrogate for the formulation (2):

$$\begin{aligned} \min_{M \in \mathcal{M}, \alpha \in [1/2, 1]} & \mathbb{P}_{X \sim \mathcal{X}_{ic}} [m_{h^M}(X) \geq \frac{1-\alpha}{\alpha}] \quad (3) \\ \text{s. t. } & \mathbb{P}_{Z \sim \mathcal{X}_{ca}} [m_{h^M}^*(Z) \geq \frac{1-\alpha}{\alpha}] \geq \beta, \end{aligned}$$

where \mathcal{X}_{ic} is the distribution formed by clean examples incorrectly classified by $h^M(\cdot)$, \mathcal{X}_{ca} is the distribution formed by attacked examples correctly classified by $h^M(\cdot)$, X, Z

are the random variables drawn from these distributions, and $\beta \in [0, 1]$ controls the desired level of robust accuracy with respect to the robust accuracy of $h(\cdot)$.

Note that (3) no longer depends on $g(\cdot)$, allowing for replacing the standard base classifier without re-solving for a new $M(\cdot)$. The following two theorems justify approximating (2) with (3) by characterizing the optimizers of (3):

Theorem 4.3. Suppose that Assumption 4.2 holds. Let r_h denote the robust accuracy of $h(\cdot)$. If $\beta \geq r_{f^M}/r_h$, then a solution to (3) is feasible for (2).

Theorem 4.4. Suppose that Assumption 4.1 holds. Furthermore, consider an input random variable X and suppose that the margin of $h^M(X)$ is independent of whether $g(X)$ is correct. Then, minimizing the objective of (3) is equivalent to maximizing the objective of (2).

The proofs to Theorems 4.3 and 4.4 are provided in Appendices A.1 and A.2, respectively. The independence assumption in Theorem 4.4 can be relaxed with minor changes to our method, which we discuss in Appendix E.3. Also note that Theorems 4.3 and 4.4 rely on using $T = 0$ for the temperature scaling for $g(\cdot)$, justifying this selection.

4.2. Parameterizing the Transformation M

Optimizing the nonlinear transformation $M(\cdot)$ requires representing it with parameters. To avoid introducing additional training requirements or vulnerable backdoors, the parameterization should be simple (*i.e.*, not introducing yet another neural network). Thus, we introduce a manually designed transformation with only three parameters, along with an algorithm to efficiently optimize the three parameters.

Unlike linear scaling and the Softmax operation, which are shift-agnostic (*i.e.*, adding a constant to all logits does not change the predicted probabilities), the desired nonlinear transformations' behavior heavily depends on the numerical range of the logits. Thus, to make the nonlinear transformation controllable and interpretable, we pre-process the logits by applying layer normalization (LN): for each input x , we standardize the logits $h(x)$ to have zero mean and identity variance. We observe that LN itself also slightly increases the margin difference between correct and incorrect examples, favoring our overall formulation as shown in Figure 2. This phenomenon is further explained in Appendix E.2.

Among the post-LN logits, only those associated with confidently predicted classes can be large positive values. To take advantage of this property, we use a clamping function $\text{Clamp}(\cdot)$, such as ReLU, GELU, ELU, or SoftPlus, to bring the logits smaller than a threshold toward zero. This clamping operation can further suppress the confidence of small-margin predictions while preserving large-margin predictions. Since correct examples often enjoy larger margins, the clamping function enlarges the margin gap between cor-

rect and incorrect examples. We provide an ablation study over candidate clamping functions in Appendix D.3 and empirically select GELU for our experiments.

Finally, since the power functions with greater-than-one exponents diminish smaller inputs while amplifying larger ones, we exponentiate the clamping function outputs to a constant power and preserve the sign. The combined nonlinearly transformed robust base classifier $h^{M_p^s}(\cdot)$ becomes

$$\begin{aligned} h^{\text{Clamp}, c}(x) &= \text{Clamp}(\text{LN}(h(x)) + c) \\ h^{M_p^s}(x) &= s \cdot |h^{\text{Clamp}, c}(x)|^p \cdot \text{sgn}(h^{\text{Clamp}, c}(x)), \end{aligned} \quad (4)$$

where $s \in (0, +\infty)$ is a scaling constant, $p \in (0, +\infty)$ is an exponent constant, and $c \in \mathbb{R}$ is a bias constant that adjusts the cutoff location of the clamping function. We apply the absolute value before the exponentiation to maintain compatibility with non-integer p values and use the sign function to preserve the sign. Note that when the clamping function is linear and $p = 1$, (4) degenerates to temperature scaling with LN. Hence, the optimal combination of s, c, p is guaranteed to be no worse than temperature scaling.

Note that the nonlinear transformation that converts $h(\cdot)$ to $h^{M_p^s}(\cdot)$ generally adheres to Assumption 4.2. While Assumption 4.2 may be slightly violated if GELU is chosen as the clamping function due to its portion around zero being not monotonic, its effect is empirically very small according to our observation, partly because the negative slope is very shallow. We additionally note that the certified robustness results presented in (Bai et al., 2023a) also apply to the nonlinearly mixed classifiers in this work.

4.3. Efficient Algorithm for Optimizing s, p, c , and α

With the nonlinear transformation parameterization in place, the functional-space optimization problem (3) reduces to the following algebraic optimization formulation:

$$\begin{aligned} \min_{s, p, c, \alpha \in \mathbb{R}} \quad & \mathbb{P}_{X \sim \mathcal{X}_{ic}} [m_{h^{M_p^s}}(X) \geq \frac{1-\alpha}{\alpha}] \\ \text{s. t.} \quad & \mathbb{P}_{Z \sim \mathcal{X}_{ca}} [m_{h^{M_p^s}}^*(Z) \geq \frac{1-\alpha}{\alpha}] \geq \beta, \\ & s \geq 0, \quad p \geq 0, \quad 1/2 \leq \alpha \leq 1. \end{aligned} \quad (5)$$

Exactly solving (5) involves evaluating $m_{h^{M_p^s}}^*(x)$ for every x in the support of \mathcal{X}_{ca} , which is intractable since the support is a continuous set and \mathcal{X}_{ca} and \mathcal{X}_{ic} implicitly depend on the optimization variables s, p , and c . To this end, we approximate \mathcal{X}_{ic} and \mathcal{X}_{ca} with a small set of data. Consider the subset of clean examples in this set incorrectly classified by $h^{\text{LN}}(\cdot)$, denoted as $\tilde{\mathcal{X}}_{ic}$, and the subset of attacked examples correctly classified by $h^{\text{LN}}(\cdot)$, denoted as $\tilde{\mathcal{X}}_{ca}$. Using them as surrogates to \mathcal{X}_{ic} and \mathcal{X}_{ca} decouples the probability measures from the optimization variables.

Despite optimizing s, p, c , and α on a small set of data, overfitting is unlikely since there are only four parameters, and

thus a small number of images should suffice. Appendix D.2 analyzes the effect of the data subset size on optimization quality and confirms the absence of overfitting.

The minimum margin $\underline{m}_{h^{M_p^s}}^*(x)$ also depends on the optimization variables s, p, c , and α , as its calculation requires the minimum-margin perturbation for $h^{M_p^s}(\cdot)$ around x . Since finding $\underline{m}_{h^{M_p^s}}^*(x)$ for all s, p , and c combinations is intractable, we seek to use an approximation that does not depend on s, p , and c . To this end, we approximate $\underline{m}_{h^{M_p^s}}^*(x)$, defined as $m_{h^{M_p^s}}(x + \delta_{h^{M_p^s}}^*(x))$, with the quantity

$$\tilde{m}_{h^{M_p^s}}(x) := m_{h^{M_p^s}}(x + \tilde{\delta}_{h^{\text{LN}}}(x)),$$

where $\tilde{\delta}_{h^{\text{LN}}}(x)$ is an empirical minimum-margin perturbation of $h^{\text{LN}}(\cdot)$ around x obtained from a strong adversarial attack. For this purpose, in Appendix B.1, we propose *minimum-margin AutoAttack (MMAA)*, an AutoAttack variant that keeps track of the minimum margin while generating perturbations. Note that calculating $\tilde{m}_{h^{M_p^s}}(x)$ does not require attacking $h^{M_p^s}(\cdot)$ but instead attacks $h^{\text{LN}}(\cdot)$, which is independent of the optimization variables.

Since the probability measures and the perturbations are now both decoupled from s, p, c, α , we only need to run MMAA once to estimate the worst-case perturbation, making this hyperparameter search problem efficiently solvable. While using $h^{\text{LN}}(\cdot)$ as a surrogate to $h^{M_p^s}(\cdot)$ introduces a distribution mismatch, we expect this mismatch to be benign. To understand this, observe that the nonlinear logit transformation (4) generally preserves the predicted class due to the (partially) monotonic characteristics of GELU and the sign-preserving power function. Consequently, we expect the accuracy and minimum-margin perturbations of $h^{M_p^s}(\cdot)$ to be very similar to those of $h^{\text{LN}}(\cdot)$. Appendix E.4 empirically verifies this speculated proximity.

To simplify notations, let $\tilde{\mathcal{A}}_{ca} := \{x + \tilde{\delta}_{h^{\text{LN}}}(x) : x \in \tilde{\mathcal{X}}_{ca}\}$ denote all correctly predicted minimum-margin perturbed images for h^{LN} . Inherently, $\mathbb{P}_{Z \in \tilde{\mathcal{A}}_{ca}} [m_{h^{M_p^s}}(Z) \geq \frac{1-\alpha}{\alpha}]$ equals to $\mathbb{P}_{Z \in \tilde{\mathcal{X}}_{ca}} [\tilde{m}_{h^{M_p^s}}(Z) \geq \frac{1-\alpha}{\alpha}]$, which then approximates $\mathbb{P}_{Z \sim \mathcal{X}_{ca}} [m_{h^{M_p^s}}^*(Z) \geq \frac{1-\alpha}{\alpha}]$. The approximate hyperparameter selection problem is then

$$\begin{aligned} \min_{s, p, c, \alpha \in \mathbb{R}} \quad & \mathbb{P}_{X \sim \tilde{\mathcal{X}}_{ic}} [m_{h^{M_p^s}}(X) \geq \frac{1-\alpha}{\alpha}] \\ \text{s. t.} \quad & \mathbb{P}_{Z \in \tilde{\mathcal{A}}_{ca}} [m_{h^{M_p^s}}(Z) \geq \frac{1-\alpha}{\alpha}] \geq \beta, \\ & s \geq 0, \quad p \geq 0, \quad 1/2 \leq \alpha \leq 1. \end{aligned} \quad (6)$$

Since (6) only has four optimization variables, it can be solved via a grid search algorithm. Furthermore, the constraint $\mathbb{P}_{Z \in \tilde{\mathcal{A}}_{ca}} [m_{h^{M_p^s}}(Z) \geq \frac{1-\alpha}{\alpha}] \geq \beta$ should always be active at optimality. To understand this, suppose that for some combination of s, p, c , and α , this inequality is satisfied strictly. Then, it will be possible to decrease α (i.e., increase $\frac{1-\alpha}{\alpha}$) without violating this constraint, and thereby

Algorithm 1 Algorithm for optimizing s , p , c , and α .

```

1: Given an image set, save the predicted logits associated with
   mispredicted clean images  $\{h^{\text{LN}}(x) : x \in \tilde{\mathcal{X}}_{ic}\}$ .
2: Run MMA on  $h^{\text{LN}}(\cdot)$  and save the logits of correctly classified
   perturbed inputs  $\{h^{\text{LN}}(x) : x \in \tilde{\mathcal{A}}_{ca}\}$ .
3: Initialize candidate values  $s_1, \dots, s_l, p_1, \dots, p_m, c_1, \dots, c_n$ .
4: for  $s_i$  for  $i = 1, \dots, l$  do
5:   for  $p_j$  for  $j = 1, \dots, m$  do
6:     for  $c_k$  for  $k = 1, \dots, n$  do
7:       Obtain mapped logits  $\{h^{M_{\beta_k}}(x) : x \in \tilde{\mathcal{A}}_{ca}\}$ .
8:       Calculate the margins from the mapped logits
    $\{m_{h^{M_{\beta_k}}}(x) : x \in \tilde{\mathcal{A}}_{ca}\}$ .
9:       Store the bottom  $1 - \beta$ -quantile of the margins as
    $q_{1-\beta}^{ijk}$  (corresponds to  $\frac{1-\alpha}{\alpha}$  in (6)).
10:      Record the current objective  $o^{ijk} \leftarrow$ 
    $\mathbb{P}_{X \in \tilde{\mathcal{X}}_{ic}} [m_{h^{M_{\beta_k}}}(X) \geq q_{1-\beta}^{ijk}]$ .
11:    end for
12:  end for
13: end for
14: Find optimal indices  $(i^*, j^*, k^*) = \arg \min_{i,j,k} o^{ijk}$ .
15: Recover optimal mixing weight  $\alpha^* := 1/(1+q_{1-\beta}^{i^* j^* k^*})$ .
16: return  $s^* := s_{i^*}, p^* := p_{j^*}, c^* := c_{k^*}, \alpha^*$ .

```

decrease the objective function. Hence, we can treat this constraint as equality, reducing the degrees of freedom to three. Specifically, we sweep over a range of s , p , and c to form a three-dimensional grid, and select the α value that binds the chance constraint. Then, we select an s , p , c combination that minimizes the objective from this grid.

The resulting algorithm is Algorithm 1. As discussed above, this algorithm only needs to query MMAA's APGD components once on a small set of data, and all other steps are simple mathematical operations. Hence, Algorithm 1 is efficiently solvable. Also note that it is not necessary to solve (6) to a very high accuracy due to the discrete nature of the approximated objective function. Thus, the number of candidate values for s , p , and c can be small, and Algorithm 1 is highly efficient despite the triply nested loop structure. Appendix D.2 reports the run time of Algorithm 1.

5. Experiments

We use extensive experiments to demonstrate the accuracy-robustness balance achieved by the MixedNUTS classifier

$$f^{M_{\beta^*}^{s^*}}(x) := \log((1 - \alpha)g^{\text{TS},0}(x) + \alpha h^{M_{\beta^*}^{s^*}}(x)), \quad (7)$$

especially focusing on the effectiveness of the nonlinear logit transformation. We validate our proposed method on the CIFAR-10 (Krizhevsky, 2012), CIFAR-100 (Krizhevsky, 2012), and ImageNet (Deng et al., 2009) datasets. For each dataset, we select the corresponding state-of-the-art model with the highest robust accuracy verified on Robust-Bench (Croce et al., 2020) as the robust base classifier $h(\cdot)$, and select a state-of-the-art standard (non-robust) model

enhanced with extra training data as the accurate base classifier $g(\cdot)$. All mixed classifiers are evaluated with a custom strengthened adaptive AutoAttack algorithm specialized in attacking MixedNUTS and do not manifest gradient obfuscation issues, with the details explained in Appendix B.2.

5.1. Main Experiment Results

The comparisons among Robust Base Classifier (RBC), Accurate Base Classifier (ABC), as well as the baseline method Mixed (Bai et al., 2023b) on the three datasets are shown in Figure 1. The results confirm that MixedNUTS consistently achieves higher clean accuracy and better robustness than a mixed classifier without the nonlinear logit transformation, demonstrating that the transformation mitigates the accuracy-robustness trade-off. By quantitatively comparing MixedNUTS with its robust base classifier $h(\cdot)$, Table 2 shows that mixing classifiers with the nonlinear transformation significantly reduces the clean error rate while incurring a small robust error rate increase. Clearly, MixedNUTS balances accuracy and robustness *without additional training*.

Meanwhile, Figure 2 compares the robust base classifier's confidence margins on clean and attacked data with or without our nonlinear logit transformation (4). For each dataset, the transformation enlarges the margin gap between correct and incorrect predictions, especially in terms of the median which represents the margin majority. Using $h^{M_{\beta^*}^{s^*}}(\cdot)$ instead of $h(\cdot)$ makes correct predictions more confident while keeping the mispredictions less confident, making the mixed classifier more accurate without losing robustness.

With the nonlinear transformation in place, it is still possible to adjust the emphasis between clean and robust accuracy at inference time. This can be achieved by simply re-running Algorithm 1 with a different β value. Note that the MMAA step in Algorithm 1 does not depend on β , and hence can be cached to speed up re-runs. Meanwhile, the computational cost of the rest of Algorithm 1 is marginal. Our experiments use $\beta = 98.5\%$ for CIFAR-10 and -100, and use $\beta = 99.0\%$ for ImageNet. The optimal s , p , c values and the searching grid used in Algorithm 1 are discussed in Appendix E.1.

Table 1 compares MixedNUTS with existing methods that achieve the best AutoAttack-validated adversarial robustness. MixedNUTS noticeably improves clean accuracy while still maintaining competitive robustness. Note that since MixedNUTS can use existing or future improved accurate or robust models as base classifiers, the entries of Table 1 should not be regarded as pure competitors.

Existing models suffer from the most pronounced accuracy-robustness trade-off on CIFAR-100, where MixedNUTS offers the most prominent improvement, boosting the clean accuracy by 7.86 percentage points over the state-of-the-art non-mixing robust model while reducing merely 0.87

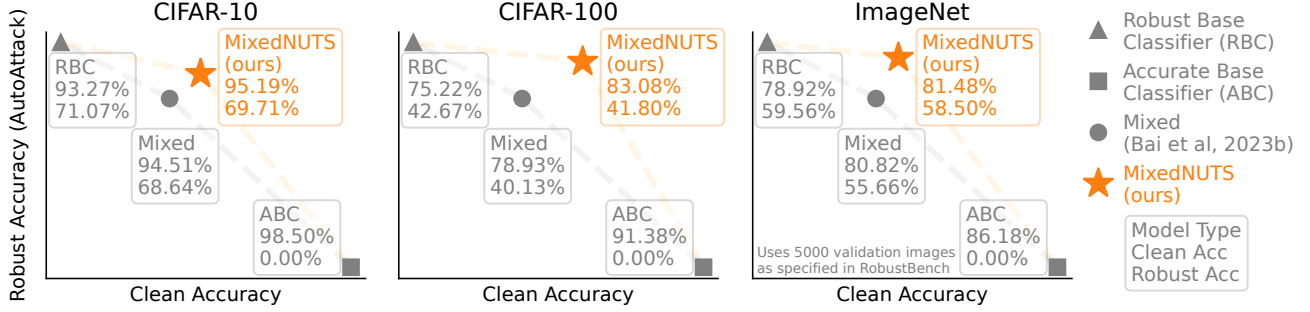


Figure 1: MixedNUTS balances the robustness from its robust base classifier and the accuracy from its standard base classifier. The nonlinear logit transformation helps MixedNUTS achieve a much better accuracy-robust trade-off than a baseline mixed model without transformation. Appendix E.1 reports the base model details and the optimal s, p, c, α values.

Table 1: MixedNUTS’s accuracy compared with state-of-the-art classifiers. “AA” abbreviates AutoAttacked accuracy.

CIFAR-10				CIFAR-100				ImageNet			
Model	Mixed	Clean (\uparrow)	AA (\uparrow)	Model	Mixed	Clean (\uparrow)	AA (\uparrow)	Model	Mixed	Clean (\uparrow)	AA (\uparrow)
This work	✓	95.19%	69.71%	This work	✓	83.08%	41.80%	This work	✓	81.48%	58.50%
Peng et al. (2023)	✗	93.27%	71.07%	Wang et al. (2023)	✗	75.22%	42.67%	Liu et al. (2023)	✗	78.92%	59.56%
Bai et al. (2023a)	✓	95.23%	68.06%	Bai et al. (2023a)	✓	85.21%	38.72%	Singh et al. (2023)	✗	77.00%	57.70%
Rebuffi et al. (2021)	✗	92.23%	66.58%	Gowal et al. (2020)	✗	69.15%	36.88%	Peng et al. (2023)	✗	73.44%	48.94%
Kolesnikov et al. (2020)	✗	98.50%	0.00%	Kolesnikov et al. (2020)	✗	91.38%	0.00%	Woo et al. (2023)	✗	86.18%	0.00%

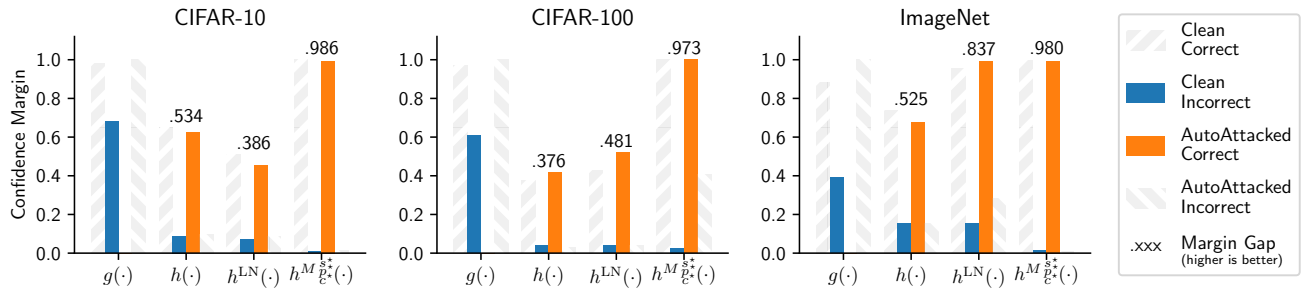


Figure 2: The median confidence margin of the accurate/robust base classifier $g(\cdot)/h(\cdot)$, the layer-normed logits $h^{LN}(\cdot)$, and the nonlinearly transformed model $h^{M_{\mathcal{P}_c^*}}(\cdot)$ on clean and AutoAttacked data, grouped by prediction correctness. The number above each bar group is the “margin gap”, defined as the difference between the medians on clean incorrect inputs and AutoAttacked correct ones. A higher margin gap signals more benign confidence property, and thus better accuracy-robustness trade-off for the mixed classifier.

Table 2: MixedNUTS’s error rate change relative to the robust base classifier (more negative is better).

	Clean (\downarrow)	Robust (AutoAttack) (\downarrow)
CIFAR-10	-28.53%	+4.70%
CIFAR-100	-31.72%	+1.52%
ImageNet	-12.14%	+2.62%

points in robust accuracy. In comparison, the previous mixing method (Bai et al., 2023a) sacrifices 3.95 points of robustness (4.5x MixedNUTS’s degradation) to achieve a 9.99-point clean accuracy bump using the same set of base models. Moreover, (Bai et al., 2023a) requires training an additional mixing network component, whereas Mixed-

NUTS is training-free (MixedNUTS is also compatible with the mixing network for even better results). Clearly, MixedNUTS utilizes the robustness of $h(\cdot)$ more effectively and efficiently. On CIFAR-10 and ImageNet, achieving robustness against the common attack budget ($8/255$ and $4/255$ respectively) penalizes the clean accuracy less severely than on CIFAR-100. Nonetheless, MixedNUTS is still effective in these less suitable cases, reducing the clean error rate by 28.53%/12.14% (relative) while only sacrificing 1.91%/0.98% (relative) robust accuracy on CIFAR-10/ImageNet compared to non-mixing methods. On CIFAR-10, MixedNUTS matches (Bai et al., 2023a)’s clean accuracy while reducing the robust error rate by 5.17% (relative).

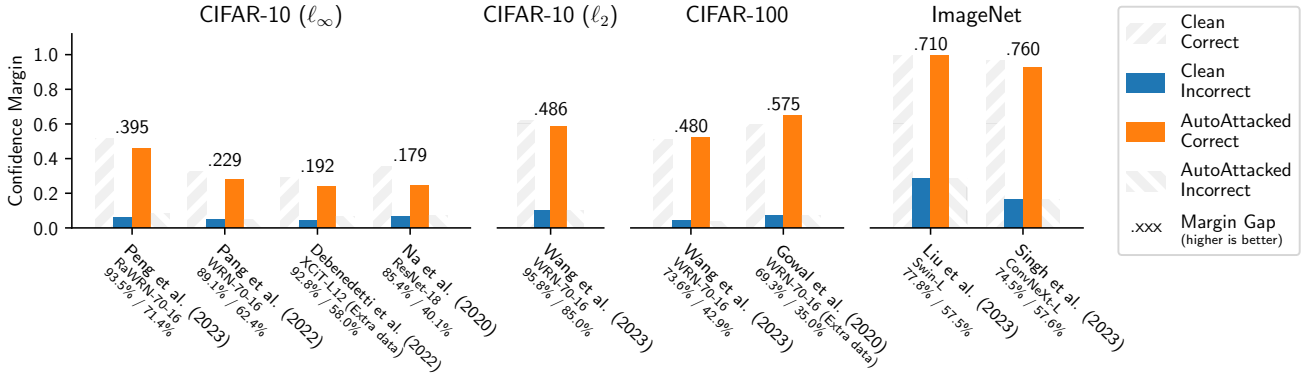


Figure 3: The median confidence margin of a diverse set of existing robust models with the logits standardized via layer normalization. These models all enjoy higher margins on correct predictions than on incorrect ones, for clean and adversarial inputs alike. The percentages below each model name are the clean/AutoAttacked accuracy.

5.2. Confidence Properties of Various Robust Models

MixedNUTS is built upon the observation that robust models are more confident in correct predictions than incorrect ones. Figure 3 confirms this property across existing models with diverse structures trained with different loss functions across various datasets, and hence MixedNUTS is applicable for a wide range of base model combinations. For a fair confidence margin comparison, all logits are standardized to zero mean and identity variance (corresponding to $h^{\text{LN}}(\cdot)$) before converted to probabilities. Appendix C.1 presents histograms to offer more margin distribution details.

Figure 3 illustrates that existing CIFAR-10 and -100 models have tiny confidence margins for mispredictions and moderate margins for correct predictions, implying that most mispredictions have a close runner-up class. Compared to CIFAR models, ImageNet classifiers have higher overall margins, with the property of more confidence in correct predictions than incorrect ones still present. Since the logits are standardized before Softmax, the higher overall confidence suggests that ImageNet models often do not have a strong confounding class despite having more classes, and their non-predicted classes’ probabilities spread more evenly.

5.3. Accuracy-Robustness Trade-Off Curves

Figure 4 displays the robust accuracy of MixedNUTS as a function of its clean accuracy and compares this accuracy-robustness trade-off curve with that of the mixed classifier without nonlinear logit transformation (as designed in (Bai et al., 2023b)) and that of TRADES, a popular adjustable method that aims to improve the trade-off (Zhang et al., 2019). For TRADES, adjusting between accuracy and robustness requires modifying a β_{TR} parameter in the loss function and training a new model. Figure 4 selects CIFAR-10 WRN-34-10 models trained with $\beta_{\text{TR}} = 0, 0.1, 0.3, 6$, where 0 corresponds to standard (non-robust) training and 6

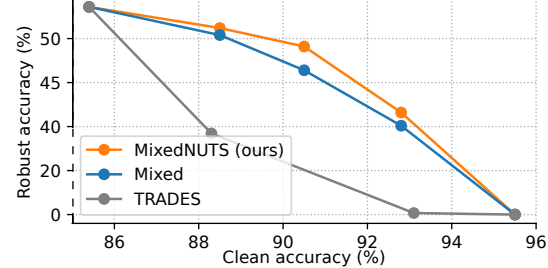


Figure 4: Accuracy-robustness trade-off comparison between MixedNUTS, mixed classifier without nonlinear transformation, and TRADES on 1000 CIFAR-10 images.

achieves the best robustness. For a fair comparison, we select the models with $\beta_{\text{TR}} = 0$ and 6 as the mixed classifiers’ base models. Figure 4 confirms that both mixed classifiers achieve much more benign trade-offs than TRADES without re-training the model. Furthermore, MixedNUTS balances accuracy and robustness better than (Bai et al., 2023b).

6. Conclusions

This work proposes MixedNUTS, a versatile training-free method that combines the output probabilities of a robust classifier and an accurate classifier. By introducing nonlinear base model logit transformations, MixedNUTS more effectively exploits the benign confidence property of the robust base classifier, thereby achieving a balance between clean data classification accuracy and adversarial robustness. For performance-driven practitioners, this balance implies less to lose in using robust models, incentivizing the real-world deployment of safe deep learning systems. For researchers, as improving the accuracy-robustness trade-off with a single model becomes harder, MixedNUTS identifies building base models with better margin properties as an alternative to improve the trade-off in an ensemble setting.

References

Adam, G. and Speciel, R. Evaluating ensemble robustness against adversarial attacks. *arXiv preprint arXiv:2005.05750*, 2020.

Alam, M., Datta, S., Mukhopadhyay, D., Mondal, A., and Chakrabarti, P. P. Resisting adversarial attacks in deep neural networks using diverse decision boundaries. *arXiv preprint arXiv:2208.08697*, 2022.

Andriushchenko, M., Croce, F., Flammarion, N., and Hein, M. Square attack: A query-efficient black-box adversarial attack via random search. In *European Conference on Computer Vision*, 2020.

Athalye, A., Engstrom, L., Ilyas, A., and Kwok, K. Synthesizing robust adversarial examples. In *International Conference on Machine Learning*, 2018.

Bai, Y., Gautam, T., Gai, Y., and Sojoudi, S. Practical convex formulation of robust one-hidden-layer neural network training. In *American Control Conference*, 2022.

Bai, Y., Anderson, B. G., Kim, A., and Sojoudi, S. Improving the accuracy-robustness trade-off of classifiers via adaptive smoothing. *arXiv preprint arXiv:2301.12554*, 2023a.

Bai, Y., Anderson, B. G., and Sojoudi, S. Mixing classifiers to alleviate the accuracy-robustness trade-off. *arXiv preprint arXiv:2311.15165*, 2023b.

Bai, Y., Gautam, T., and Sojoudi, S. Efficient global optimization of two-layer relu networks: Quadratic-time algorithms and adversarial training. *SIAM Journal on Mathematics of Data Science*, 2023c.

Balaji, Y., Goldstein, T., and Hoffman, J. Instance adaptive adversarial training: Improved accuracy tradeoffs in neural nets. *arXiv preprint arXiv:1910.08051*, 2019.

Borkar, J. and Chen, P.-Y. Simple transparent adversarial examples. *arXiv preprint arXiv:2105.09685*, 2021.

Carlini, N. and Wagner, D. A. Towards evaluating the robustness of neural networks. In *IEEE Symposium on Security and Privacy*, 2017.

Chen, T., Zhang, Z., Liu, S., Chang, S., and Wang, Z. Robust overfitting may be mitigated by properly learned smoothening. In *International Conference on Learning Representations*, 2020.

Cheng, M., Lei, Q., Chen, P. Y., Dhillon, I., and Hsieh, C. J. CAT: Customized adversarial training for improved robustness. In *International Joint Conference on Artificial Intelligence*, 2022.

Co, K. T., Martinez-Rego, D., Hau, Z., and Lupu, E. C. Jacobian ensembles improve robustness trade-offs to adversarial attacks. In *Artificial Neural Networks and Machine Learning*, 2022.

Croce, F. and Hein, M. Reliable evaluation of adversarial robustness with an ensemble of diverse parameter-free attacks. In *International Conference on Machine Learning*, 2020.

Croce, F., Andriushchenko, M., Sehwag, V., Debenedetti, E., Flammarion, N., Chiang, M., Mittal, P., and Hein, M. Robustbench: a standardized adversarial robustness benchmark. *arXiv preprint arXiv:2010.09670*, 2020.

Cui, J., Tian, Z., Zhong, Z., Qi, X., Yu, B., and Zhang, H. Decoupled kullback-leibler divergence loss. *arXiv preprint arXiv:2305.13948*, 2023.

Debenedetti, E., Sehwag, V., and Mittal, P. A light recipe to train robust vision transformers. *arXiv preprint arXiv:2209.07399*, 2022.

Deng, J., Dong, W., Socher, R., Li, L.-J., Li, K., and Fei-Fei, L. ImageNet: A large-scale hierarchical image database. In *IEEE Conference on Computer Vision and Pattern Recognition*, 2009.

Ganaie, M. A., Hu, M., Malik, A., Tanveer, M., and Suganthan, P. Ensemble deep learning: A review. *Engineering Applications of Artificial Intelligence*, 115:105151, 2022.

Goodfellow, I. J., Shlens, J., and Szegedy, C. Explaining and harnessing adversarial examples. In *International Conference on Learning Representations*, 2015.

Gowal, S., Uesato, J., Qin, C., Huang, P.-S., Mann, T., and Kohli, P. An alternative surrogate loss for pgd-based adversarial testing. *arXiv preprint arXiv:1910.09338*, 2019.

Gowal, S., Qin, C., Uesato, J., Mann, T., and Kohli, P. Uncovering the limits of adversarial training against norm-bounded adversarial examples. *arXiv preprint arXiv:2010.03593*, 2020.

Gowal, S., Rebuffi, S.-A., Wiles, O., Stimberg, F., Calian, D. A., and Mann, T. Improving robustness using generated data. *arXiv preprint arXiv:2110.09468*, 2021.

Guo, C., Pleiss, G., Sun, Y., and Weinberger, K. Q. On calibration of modern neural networks. In *International Conference on Machine Learning*, 2017.

Hinton, G., Vinyals, O., and Dean, J. Distilling the knowledge in a neural network. *arXiv preprint arXiv:1503.02531*, 2015.

Ilyas, A., Engstrom, L., Athalye, A., and Lin, J. Black-box adversarial attacks with limited queries and information. In *International Conference on Machine Learning*, 2018.

Kolesnikov, A., Beyer, L., Zhai, X., Puigcerver, J., Yung, J., Gelly, S., and Houlsby, N. Big transfer (BiT): General visual representation learning. In *European Conference on Computer Vision*, 2020.

Krizhevsky, A. Learning multiple layers of features from tiny images. <https://www.cs.toronto.edu/~kriz/learning-features-2009-TR.pdf>, 2012.

Li, L., Wang, Y., Sitawarin, C., and Spratling, M. Oodrobustbench: benchmarking and analyzing adversarial robustness under distribution shift. *arXiv preprint arXiv:2310.12793*, 2023.

Liu, C., Dong, Y., Xiang, W., Yang, X., Su, H., Zhu, J., Chen, Y., He, Y., Xue, H., and Zheng, S. A comprehensive study on robustness of image classification models: Benchmarking and rethinking. *arXiv preprint arXiv:2302.14301*, 2023.

Liu, F. and Zhao, R. Towards both accurate and robust neural networks without extra data. In *International Conference on Artificial Neural Networks*, 2022.

Liu, J., Paisley, J., Kioumourtzoglou, M.-A., and Coull, B. Accurate uncertainty estimation and decomposition in ensemble learning. In *Advances in Neural Information Processing Systems*, 2019.

Madry, A., Makelov, A., Schmidt, L., Tsipras, D., and Vladu, A. Towards deep learning models resistant to adversarial attacks. In *International Conference on Learning Representations*, 2018.

Na, D. Pytorch adversarial training on cifar-10. <https://github.com/nalj796/Pytorch-Adversarial-Training-CIFAR>, 2020.

Pang, T., Xu, K., Du, C., Chen, N., and Zhu, J. Improving adversarial robustness via promoting ensemble diversity. In *International Conference on Machine Learning*, 2019.

Pang, T., Lin, M., Yang, X., Zhu, J., and Yan, S. Robustness and accuracy could be reconcilable by (proper) definition. *arXiv preprint arXiv:2202.10103*, 2022.

Papernot, N., McDaniel, P., Goodfellow, I., Jha, S., Celik, Z. B., and Swami, A. Practical black-box attacks against machine learning. In *ACM Asia Conference on Computer and Communications Security*, 2017.

Peng, S., Xu, W., Cornelius, C., Hull, M., Li, K., Duggal, R., Phute, M., Martin, J., and Chau, D. H. Robust principles: Architectural design principles for adversarially robust CNNs. *arXiv preprint arXiv:2308.16258*, 2023.

Petrov, A., Eiras, F., Sanyal, A., Torr, P. H., and Bibi, A. Certifying ensembles: A general certification theory with S-Lipschitzness. *arXiv preprint arXiv:2304.13019*, 2023.

Rade, R. and Moosavi-Dezfooli, S.-M. Helper-based adversarial training: Reducing excessive margin to achieve a better accuracy vs. robustness trade-off. In *ICML 2021 Workshop on Adversarial Machine Learning*, 2021.

Raghunathan, A., Xie, S. M., Yang, F., Duchi, J. C., and Liang, P. Understanding and mitigating the tradeoff between robustness and accuracy. In *International Conference on Machine Learning*, 2020.

Rebuffi, S.-A., Gowal, S., Calian, D. A., Stimberg, F., Wiles, O., and Mann, T. Fixing data augmentation to improve adversarial robustness. *arXiv preprint arXiv:2103.01946*, 2021.

Sehwag, V., Mahloujifar, S., Handina, T., Dai, S., Xiang, C., Chiang, M., and Mittal, P. Robust learning meets generative models: Can proxy distributions improve adversarial robustness? In *International Conference on Learning Representations*, 2022.

Shafahi, A., Najibi, M., Ghiasi, M. A., Xu, Z., Dickerson, J., Studer, C., Davis, L. S., Taylor, G., and Goldstein, T. Adversarial training for free! In *Annual Conference on Neural Information Processing Systems*, 2019.

Singh, N. D., Croce, F., and Hein, M. Revisiting adversarial training for imagenet: Architectures, training and generalization across threat models. *arXiv preprint arXiv:2303.01870*, 2023.

Tramèr, F., Carlini, N., Brendel, W., and Madry, A. On adaptive attacks to adversarial example defenses. In *Annual Conference on Neural Information Processing Systems*, 2020.

Tsipras, D., Santurkar, S., Engstrom, L., Turner, A., and Madry, A. Robustness may be at odds with accuracy. In *International Conference on Learning Representations*, 2019.

Wang, Z., Pang, T., Du, C., Lin, M., Liu, W., and Yan, S. Better diffusion models further improve adversarial training. *arXiv preprint arXiv:2302.04638*, 2023.

Woo, S., Debnath, S., Hu, R., Chen, X., Liu, Z., Kweon, I. S., and Xie, S. ConvNeXt V2: Co-designing and scaling convnets with masked autoencoders. In *IEEE/CVF Conference on Computer Vision and Pattern Recognition*, 2023.

Yang, Z., Li, L., Xu, X., Kailkhura, B., Xie, T., and Li, B. On the certified robustness for ensemble models and beyond. In *International Conference on Learning Representations*, 2022.

Yu, Y., Bates, S., Ma, Y., and Jordan, M. Robust calibration with multi-domain temperature scaling. 2022.

Zhang, H., Yu, Y., Jiao, J., Xing, E. P., Ghaoui, L. E., and Jordan, M. I. Theoretically principled trade-off between robustness and accuracy. In *International Conference on Machine Learning*, 2019.

A. Proofs

A.1. Proof to Theorem 4.3

Theorem 4.3 (restated). Suppose that Assumption 4.2 holds. Let r_h denote the robust accuracy of $h(\cdot)$. If $\beta \geq r_{f^M}/r_h$, then a solution to (3) is feasible for (2).

Proof. Suppose that $M(\cdot)$ is a solution from (3). Since the mixed classifier $f^M(\cdot)$ is by construction guaranteed to be correct and robust at some x if $h^M(\cdot)$ is correct and robust with a margin no smaller than $\frac{1-\alpha}{\alpha}$ at x , it holds that

$$\begin{aligned} \mathbb{P}_{(X,Y) \sim \mathcal{D}} \left[\arg \max_i f_i^M(X + \delta_{f^M}^*(X)) = Y \right] &\geq \mathbb{P}_{(X,Y) \sim \mathcal{D}} \left[m_{h_i^M}(X + \delta_{f^M}^*(X)) \geq \frac{1-\alpha}{\alpha}, H_{\text{cor}}(X) \right] \\ &= \mathbb{P}_{(X,Y) \sim \mathcal{D}} \left[m_{h_i^M}(X + \delta_{f^M}^*(X)) \geq \frac{1-\alpha}{\alpha} \mid H_{\text{cor}}^M(X) \right] \cdot \mathbb{P}_{(X,Y) \sim \mathcal{D}} [H_{\text{cor}}^M(X)], \end{aligned}$$

where $H_{\text{cor}}(X)$ denotes the event of $h(\cdot)$ being correct at X , i.e., $\arg \max_i h_i(X + \delta_{f^M}^*(X)) = Y$. Similarly, $H_{\text{cor}}^M(X)$ denotes $\arg \max_i h_i^M(X + \delta_{f^M}^*(X)) = Y$. Under Assumption 4.2, $H_{\text{cor}}(X)$ is equivalent to $H_{\text{cor}}^M(X)$. Therefore,

$$\begin{aligned} \mathbb{P}_{(X,Y) \sim \mathcal{D}} \left[\arg \max_i f_i^M(X + \delta_{f^M}^*(X)) = Y \right] &= \mathbb{P}_{(X,Y) \sim \mathcal{D}} \left[m_{h_i^M}(X + \delta_{f^M}^*(X)) \geq \frac{1-\alpha}{\alpha} \mid H_{\text{cor}}(X) \right] \cdot \mathbb{P}_{(X,Y) \sim \mathcal{D}} [H_{\text{cor}}(X)] \\ &= r_h \cdot \mathbb{P}_{X \sim \mathcal{X}_{\text{ca}}} \left[m_{h_i^M}(X + \delta_{f^M}^*(X)) \geq \frac{1-\alpha}{\alpha} \right] \\ &\geq r_h \cdot \mathbb{P}_{Z \sim \mathcal{X}_{\text{ca}}} \left[\underline{m}_{h^M}^*(Z) \geq \frac{1-\alpha}{\alpha} \right] \geq r_h \cdot \beta \geq r_{f^M}, \end{aligned}$$

which proves the statement. \square

A.2. Proof to Theorem 4.4

Theorem 4.4 (restated). Suppose that Assumption 4.1 holds. Furthermore, consider an input random variable X and suppose that the margin of $h^M(X)$ is independent of whether $g(X)$ is correct. Then, minimizing the objective of (3) is equivalent to maximizing the objective of (2).

Proof. By construction, for an clean input x incorrectly classified by $h^M(\cdot)$, i.e., x is in the support of \mathcal{X}_{ic} , the mixed classifier prediction $f(x)$ is correct if and only if $g^{\text{TS},0}(x)$ is correct and $h^M(x)$'s margin is no greater than $\frac{1-\alpha}{\alpha}$. Let $G_{\text{cor}}(X)$ denote the event of $g(X)$ being correct, i.e., $\arg \max_i g^{\text{TS},0}(X) = Y$. Furthermore, let \mathcal{D}_{ic} denote the data-label distribution formed by clean examples incorrectly predicted by $h^M(\cdot)$. Then,

$$\begin{aligned} \mathbb{P}_{(X,Y) \sim \mathcal{D}_{ic}} \left[\arg \max_i f_i^M(X) = Y \right] &= \mathbb{P}_{X \sim \mathcal{X}_{ic}} \left[m_{h^M}(X) < \frac{1-\alpha}{\alpha}, G_{\text{cor}}(X) \right] \\ &= \mathbb{P}_{X \sim \mathcal{X}_{ic}} \left[m_{h^M}(X) < \frac{1-\alpha}{\alpha} \mid G_{\text{cor}}(X) \right] \cdot \mathbb{P}_{X \sim \mathcal{X}_{ic}} [G_{\text{cor}}(X)] \end{aligned}$$

for all transformations M and mixing weight α (recall that $f^M(\cdot)$ depends on α).

Suppose that the margin of $h^M(\cdot)$ is independent from the accuracy of $g(\cdot)$, then the above probability further equals to

$$(1 - \mathbb{P}_{X \sim \mathcal{X}_{ic}} \left[m_{h^M}(X) \geq \frac{1-\alpha}{\alpha} \right]) \cdot \mathbb{P}_{X \sim \mathcal{X}_{ic}} [G_{\text{cor}}(X)]$$

Since $\mathbb{P}_{X \sim \mathcal{X}_{ic}} [G_{\text{cor}}(X)]$ does not depend on M or α , it holds that

$$\begin{aligned} \arg \min_{M \in \mathcal{M}, \alpha \in [1/2, 1]} \mathbb{P}_{X \sim \mathcal{X}_{ic}} \left[m_{h^M}(X) \geq \frac{1-\alpha}{\alpha} \right] &= \arg \max_{M \in \mathcal{M}, \alpha \in [1/2, 1]} \mathbb{P}_{(X,Y) \sim \mathcal{D}_{ic}} \left[\arg \max_i f_i^M(X) = Y \right] \\ &= \arg \max_{M \in \mathcal{M}, \alpha \in [1/2, 1]} \mathbb{P}_{(X,Y) \sim \mathcal{D}} \left[\arg \max_i f_i^M(X) = Y \right], \end{aligned}$$

where the last equality holds because under Assumption 4.1, $h^M(x)$ being correct guarantees $g^{\text{TS},0}(x)$'s correctness. Since $f^M(\cdot)$ must be correct when $h^M(x)$ and $g^{\text{TS},0}(x)$ are both correct, the mixed classifier must be correct at clean examples correctly classified by $h^M(\cdot)$. Hence, maximizing $f^M(\cdot)$'s clean accuracy on $h^M(\cdot)$'s mispredictions is equivalent to maximizing $f^M(\cdot)$'s overall clean accuracy. \square

B. Custom Attack Algorithms

B.1. Minimum-Margin AutoAttack

Our margin-based hyperparameter selection procedure (Algorithm 1) and confidence margin estimation experiments (Figures 2 and 3) require approximating the minimum-margin perturbations associated with the robust base classifier in order to analyze the mixed classifier behavior. Approximating these perturbations requires a strong attack algorithm. While AutoAttack is often regarded as a strong adversary that reliably evaluates model robustness, its original implementation released with (Croce & Hein, 2020) does not return all perturbed examples. Specifically, traditional AutoAttack does not record the perturbation around an input if it deems the model to be robust at this input (i.e., model prediction does not change). While this is acceptable for estimating robust accuracy, it forbids the calculation of correctly predicted AutoAttacked examples' confidence margins, which are required by Algorithm 1, Figure 2, and Figure 3.

To construct a strong attack algorithm compatible with margin estimation, we propose *minimum-margin AutoAttack (MMAA)*. Specifically, we modify the two APGD components of AutoAttack (untargeted APGD-CE and targeted APGD-DLR) to keep track of the margin at each attack step (the margin history is shared across the two components) and always return the perturbation achieving the smallest margin. The FAB and Square components of AutoAttack are much slower than the two APGD components, and for our base classifiers, FAB and Square rarely succeed in altering the model predictions for images that APGD attacks fail to attack. Therefore, we exclude them for the purpose of margin estimation (but include them for the robustness evaluation of MixedNUTS).

B.2. Attacks for Nonlinearly Mixed Classifier Robustness Evaluation

When proposing a novel adversarially robust model, reliably measuring its robustness with strong adversaries is always a top priority. Hence, in addition to designing MMAA for the goal of margin estimation, we devise an adaptive attack to evaluate the robustness of the MixedNUTS and its nonlinearly mixed model defense mechanism.

Following the guidelines for constructing adaptive attacks (Tramèr et al., 2020), our adversary maintains full access to the end-to-end gradient information of the mixed classifier $f(\cdot)$. Nonetheless, when temperature scaling with $T = 0$ is applied to the accurate base classifier $g(\cdot)$ as discussed in Section 3.1, $g^{\text{TS},T}(\cdot)$ is no longer differentiable. While this is an advantage in practice since the mixed classifier becomes harder to attack, we need to circumvent this obfuscated gradient issue in our evaluations to properly demonstrate white-box robustness. To this end, transfer attack comes to the rescue. We construct an auxiliary differentiable mixed classifier $\tilde{f}(\cdot)$ by mixing $g(\cdot)$'s unmapped logits with $h^M(\cdot)$. We allow our attacks to query the gradient of $\tilde{f}(\cdot)$ to guide the gradient-based attack on $f(\cdot)$. Since $g(\cdot)$ and $g^{\text{TS},T}(\cdot)$ always produce the same predictions, the transferability between $\tilde{f}(\cdot)$ and $f(\cdot)$ should be high.

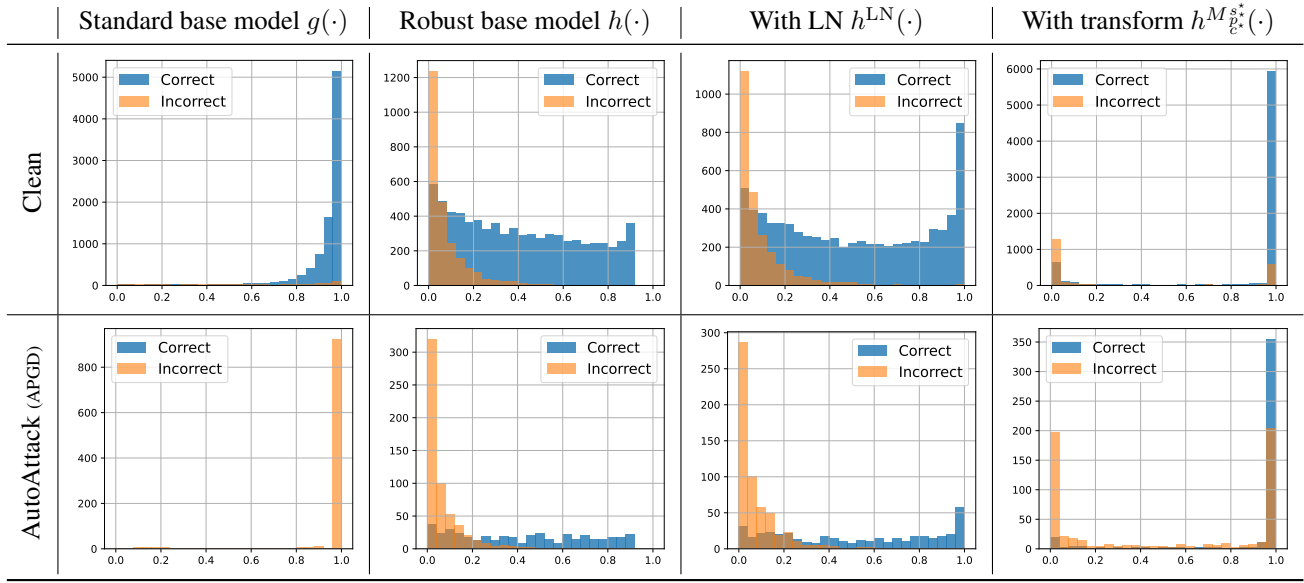
On the other hand, while $h(\cdot)$'s nonlinear logit transformation (4) is differentiable, it may also hinder gradient flow in certain cases, especially when the logits fall into the relatively flat near-zero portion of the clamping function $\text{Clamp}(\cdot)$. Hence, we also provide the raw logits of $h(\cdot)$ to our evaluation adversary for better gradient flow. To keep the adversary aware of the transformation M_c^s , we also include it in the gradient. The overall construction of the auxiliary differentiable mixed classifier $\tilde{f}(\cdot)$ is then

$$\tilde{f}(x) = \log \left((1 - \alpha_d) \sigma \circ g(\cdot) + \alpha_d r_d \sigma \circ g(\cdot) + \alpha_d (1 - r_d) \sigma \circ h^{M_c^{s*}}(\cdot) \right), \quad (8)$$

where α_d is the mixing weight and r_d adjusts the level of contribution of M_c^s to the gradient. Our experiments fix r_d to 0.9 and calculate α_d using Algorithm 1 with no clamping function, s and p fixed to 1, and c fixed to 0. The gradient-based components (APGD and FAB) of our adaptive AutoAttack use $\nabla \tilde{f}(x)$ as a surrogate for $\nabla f^{M_c^{s*}}(x)$, whereas the gradient-free Square attack component remains unchanged.

With the transfer-based gradient query in place, our adaptive AutoAttack does not suffer from gradient obfuscation, a phenomenon that leads to overestimated robustness. Specifically, we observe that the black-box Square component of our adaptive AutoAttack does not change the prediction of any images that white-box components fail to attack, confirming the effectiveness of querying the transfer-based auxiliary differentiable mixed classifier for the gradient. If we set r_d to 0 (i.e., do not bypass M_c^s for gradient), the AutoAttacked accuracy of the CIFAR-100 model reported in Figure 1 becomes 42.97% instead of 41.80%, and the black-box Square attack finds 12 vulnerable images. This comparison confirms that the proposed modifications on AutoAttack strengthen its effectiveness against MixedNUTS and eliminate the gradient flow issue, making it a reliable robustness evaluator.

Table 3: Prediction confidence margin of $h(\cdot)$, $h^{\text{LN}}(\cdot)$, and $h^{M_{\hat{v}^*}^s}(\cdot)$ used in the CIFAR-100 experiments in Figure 2. The nonlinear logit transformation (4) amplifies the margin advantage of correct predictions over incorrect ones. As in Figure 2, 10000 clean examples and 1000 AutoAttack examples are used.



C. Additional Visualizations

C.1. Confidence Margin Histograms

Table 3 displays the histograms of the confidence margins of the base classifiers used in the CIFAR-100 experiment in Figure 1. We can observe the following conclusions, which support the design of MixedNUTS:

- $g(\cdot)$ is more confident when making mistakes under attack than when correctly predicting clean images.
- $h(\cdot)$ is more confident in correct predictions than in incorrect ones, as required by MixedNUTS. Note that even when subject to strong AutoAttack, correct predictions are still more confident than incorrect predictions on clean unperturbed images.
- Layer normalization increases $h(\cdot)$ ’s correct prediction margins while maintaining the incorrect margins.
- MixedNUTS’s nonlinear logit transformation significantly boosts the correct margins while keeping most incorrect margins small.

C.2. Visualization of Transformed Probabilities

We first visualize how the proposed nonlinear transformation (4) before the Softmax operation affects the behavior of the resulting prediction probabilities. Consider a three-class classification problem, with three example $h(\cdot)$ logit vectors: $(0.9, 1.0, 1.1)$, $(-1.0, 1.1, 1.0)$, and $(1.0, -1.1, -1.0)$. The first example reflects an overall unconfident scenario, the second vector simulates the case of two competing classes, and the third example illustrates a confidently predicted instance. We then compare how the post-Softmax probability of each class changes when $h(\cdot)$ and $h^M(\cdot)$ are subject to temperature scaling. Specifically, varying the temperature scalar T from T_{\max} to T_{\min} results in probability trajectories of $\sigma(h^{M_{\hat{v}^*}^s}(\cdot)/T)$ on the probability simplex, and we compare the trajectories with those associated with $\sigma(h(\cdot)/T)$.

The four columns of Figure 5 present the trajectories obtained using different T_{\min} while fixing T_{\max} to 100. A point close to a simplex vertex signals a high-margin prediction, whereas a point close to an edge results from competing classes. The trajectories show that the nonlinear transformation increases the confidence of the first example (unconfident) while decreasing that of the second example (competing classes). Moreover, $h^{M_{\hat{v}^*}^s}(\cdot)$ ’s trajectories are overall straighter and further from the edges than $h(\cdot)$ ’s, implying rarer class competition. In the context of mixed classifiers, when $h^{M_{\hat{v}^*}^s}(\cdot)$ is used as a robust base classifier mixed with an accurate classifier $g(\cdot)$, the nonlinear transformation gives $g(\cdot)$ more relative authority when $h(\cdot)$ encounters competing classes. Such a quality improves the accuracy-robustness trade-off of the mixed classifier.

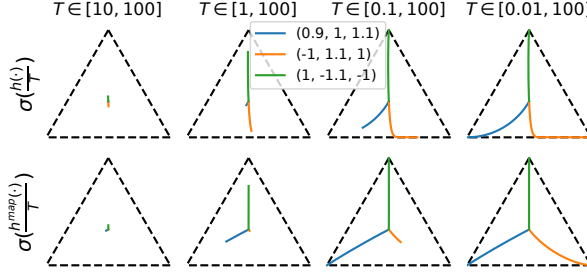


Figure 5: Prediction probability trajectories of $\sigma \circ h(\cdot)$ and $\sigma \circ h^{M_p^s}(\cdot)$ on the probability simplex. The logit transformation reduces confidence when there are competing classes.

Table 5: MixedNUTS’s clean and AutoAttack accuracy on a 1000-example CIFAR-100 subset with various temperature scales for the standard base model $g(\cdot)$. The robust base classifier is $h^{M_p^s}(\cdot)$ with the s, p, c values reported in Table 8.

Accurate Base Model	Clean	AutoAttack
$g^{\text{TS},0}(\cdot)$ (Default)	82.8%	41.6%
$g^{\text{TS},0.5}(\cdot)$	82.8%	41.4%
$g^{\text{TS},1}(\cdot)$	82.8%	41.3%

Table 6: MixedNUTS’s clean and AutoAttack accuracy when s, p , and c are optimized using different numbers of images. Evaluated with the CIFAR-100 base models from Figure 1 on a 1000-example subset.

# Images for Optimization	Clean	AutoAttack
1000 (Default)	82.8%	41.6%
300	83.0%	41.5%
100	85.1%	39.5%

Table 4: Compare several clamping functions.

Clamp(·)	s^*	c^*	p^*	α^*	β	Obj (↓)
CIFAR-10						
Linear	.050	-	9.14	.963	.985	.671
ReLU	10.4	-.750	4.00	.934	.985	.671
GELU	2.59	-.750	4.00	.997	.985	.671
CIFAR-100						
Linear	.000005	-	10.5	.880	.985	.504
ReLU	.612	-2.29	4.00	.972	.985	.500
GELU	.612	-2.14	3.57	.986	.985	.500

Table 7: The accuracy on images used for calculating s^*, p^* , and c^* (marked by \checkmark in the “Seen” column) is similar to that on images unseen by Algorithm 1 (marked by \times), confirming the absence of overfitting.

Dataset	Seen	Clean	AutoAttack
CIFAR-10	✓	95.20%	69.20%
	✗	95.18%	69.77%
CIFAR-100	✓	82.80%	41.60%
	✗	83.11%	41.82%
ImageNet	✓	82.60%	60.80%
	✗	81.20%	57.93%

D. Ablation Studies

D.1. Temperature Scaling for $g(\cdot)$

This section verifies that scaling up the logits of $g(\cdot)$ improves the accuracy-robustness trade-off of the mixed classifier. We select the pair of CIFAR-100 base classifiers used in Figure 1. By jointly adjusting the temperature of $g(\cdot)$ and the mixing weight α , we can keep the clean accuracy of the mixed model to approximately 84 percent and compare the APGD accuracy. In Table 5, we consider two temperature constants: 0.5 and 0. Note that as defined in Section 2.1, when the temperature is zero, the resulting prediction probabilities $\sigma \circ g(\cdot)$ is the one-hot vector associated with the predicted class. As demonstrated by the CIFAR-100 example in Table 5, when we fix the clean accuracy to 82.8%, using $T = 0.5$ and $T = 0$ produces higher AutoAttacked accuracy than $T = 1$ (no scaling), with $T = 0$ producing the best accuracy-robustness balance.

D.2. Run Time of Algorithm 1, Effect of Optimization Dataset Size, and Absence of Overfitting

Algorithm 1 requires performing MMAA on a set of validation images. Performing this attack on 1000 images requires 3752/10172 seconds for CIFAR-100/ImageNet with one Nvidia RTX-8000 GPU. Other steps of Algorithm 1 require minimal computation. While there is a triply-nested loop, since the number of candidate values need not be large as discussed in Section 4.3, the loops can be completed within ten seconds and can even be performed on a laptop computer.

Since the MMAA step has the dominant computational time, reducing the number of images used in Algorithm 1 can greatly accelerate it. Analyzing the effect of this data size also helps understand whether optimizing s, p , and c on validation images introduces overfitting. Table 6 shows that on CIFAR-100, reducing the number of images used in the optimization from 1000 to 300 (3 images per class) has minimal effect on the resulting mixed classifier performance. Further reducing the optimized subset size to 100 still allows for an accuracy-robustness balance, but shifts the balance towards clean accuracy.

To further demonstrate the absence of overfitting, Table 7 reports that under the default setting of optimizing s, p, c on 1000 images, the accuracy on these 1000 images is similar to that on the rest of the validation images unseen during optimization. The CIFAR-10 and -100 models, in fact, perform slightly better on unseen images. The ImageNet model’s accuracy on

unseen images is marginally lower than seen ones, likely due to the scarcity of validation images per class (only 5 per class in total since ImageNet has 1000 classes) and the resulting performance variance across the validation set.

D.3. Selecting the Clamping Function

This section performs an ablation study on the clamping function in the nonlinear logit transformation defined in (4). Specifically, we compare using GELU or ReLU as $\text{Clamp}(\cdot)$ to bypassing $\text{Clamp}(\cdot)$ (i.e., use a linear function). Here, we select a CIFAR-10 ResNet-18 model (Na, 2020) and a CIFAR-100 WideResNet-70-16 model (Wang et al., 2023) as two examples of $h(\cdot)$ and compare the optimal objective returned by Algorithm 1 using each of the clamping function settings. As shown in Table 4, while the optimal objective is similar for all three options, the returned hyperparameters s^* , p^* , c^* , and α^* is the most “modest” for GELU, which translates to the best numerical stability. In comparison, using a linear clamping function requires applying a power of 9.14 to the logits, whereas using the ReLU clamping function requires scaling the logits up by a factor of 10.4 for CIFAR-10, potentially resulting in significant numerical instabilities. Therefore, we select GELU as the default clamping function and use it for all other experiments.

D.4. Selecting the Base Classifiers

This section provides some guidelines on how to select the accurate and robust base classifiers for the best mixed classifier performance. For the accurate classifier, since MixedNUTS only considers its predicted class and does not depend on its confidence (recall that MixedNUTS uses $g^{\text{TS},0}(\cdot)$), the classifier with the best-known clean accuracy should be selected. Meanwhile, for the robust base classifier, since MixedNUTS relies on its margin properties, one should select a model that has high robust accuracy as well as benign margin characteristics (i.e., is significantly more confident in correct predictions than incorrect ones). As shown in Figure 3, most high-performance robust models share this benign property, and there is not a strong correlation between robust accuracy and margins. Therefore, state-of-the-art robust models are usually safe to use.

That being said, consider the hypothetical scenario that between a pair of robust base classifiers on some dataset, one has higher robust accuracy and the other has more benign margin properties. In this case, one should compare the percentages of data that the two models are robust at with a certain non-zero margin. The model with higher “robust accuracy with margin” should be selected.

Table 8: Details of the base classifiers used in our main experiments.

Dataset	Robust Base Classifier $g(\cdot)$	Accurate Base Classifier $h(\cdot)$
CIFAR-10	ResNet-152 (Kolesnikov et al., 2020)	RaWRN-70-16 (Peng et al., 2023)
CIFAR-100	ResNet-152 (Kolesnikov et al., 2020)	WRN-70-16 (Wang et al., 2023)
ImageNet	ConvNeXt V2-L (Woo et al., 2023)	Swin-L (Liu et al., 2023)

 Table 9: The optimal s, p, c, α values returned by Algorithm 1 used in our main experiments, presented along with the minimum and maximum candidate values in Algorithm 1’s searching grid.

	s^*	c^*	p^*	α^*	s_{\min}	s_{\max}	c_{\min}	c_{\max}	p_{\min}	p_{\max}
CIFAR-10	5.00	-1.10	4.00	.999	0.05	5	-1.1	0	1	4
CIFAR-100	.612	-2.14	3.57	.986	0.05	4	-2.5	-0.4	1	4
ImageNet	.0235	-.286	2.71	.997	0.01	0.2	-2	0	2	3

 Table 10: The proposed nonlinear logit transformation $M_{\hat{c}}^{s^*}$ has minimal effect on base model accuracy.

Dataset	Clean (full dataset)			AutoAttack (1000 images)		
	$h(\cdot)$	$h^{\text{LN}}(\cdot)$	$h^{M_{\hat{c}}^{s^*}}(\cdot)$	$h(\cdot)$	$h^{\text{LN}}(\cdot)$	$h^{M_{\hat{c}}^{s^*}}(\cdot)$
CIFAR-10	93.27%	93.27%	93.25%	71.4%	71.4%	71.4%
CIFAR-100	75.22%	75.22%	75.22%	43.0%	42.9%	43.3%
ImageNet	78.75%	78.75%	78.75%	57.5%	57.5%	57.5%

E. Additional Discussions

E.1. Base Classifier and Mixing Details in Main Experiment

Table 8 presents the sources and architectures of the base classifiers selected for our main experiments (Figure 1, Figure 2, Table 1, and Table 2). The robust base classifiers are the state-of-the-art models listed on RobustBench as of submission, and the accurate base classifiers are popular high-performance models pre-trained on large datasets. Note that since MixedNUTS only queries the predicted classes from $g(\cdot)$ and is agnostic of its other details, $g(\cdot)$ may be any classifier, including large-scale vision-language models that currently see rapid development.

Table 9 presents the optimal s^*, p^*, c^* , and α^* values used in MixedNUTS’s nonlinear logit transformation returned by Algorithm 1. When optimizing s, p , and c , Algorithm 1 performs a grid search, selecting from a provided set of candidate values. In our experiments, we generate uniform linear intervals as the candidate values for the power coefficient p and the bias coefficient c , and use a log-scale interval for the scale coefficient s . Each interval has eight numbers, with the minimum and maximum values for the intervals listed in Table 9.

Table 10 demonstrates that MixedNUTS’s nonlinear logit transformation $M_{\hat{c}}^{s^*}$ has negligible effects on base classifier accuracy, confirming that MixedNUTS’s improved accuracy-robustness balance is rooted in the improved base classifier confidence properties.

E.2. Behavior of Logit Normalization

The LN operation on the model logits makes the margin agnostic to the overall scale of the logits. Consider two example logit vectors in \mathbb{R}^3 , namely $(0.9, 1, 1.1)$ and $(-2, 1, 1.1)$. The first vector corresponds to the case where the classifier prefers the third class but is relatively unconfident. The second vector reflects the scenario where the classifier is generally more confident, but the second and third classes compete with each other. The LN operation will scale up the first vector and scale down the second. It is likely that the competing scenario is more common when the prediction is incorrect, and therefore the LN operation, which comparatively decreases the margin under the competing scenario, makes incorrect examples less confident compared with correct ones. As a result, the LN operation itself can slightly enlarge the margin difference between incorrect and correct examples.

For ImageNet, instead of performing LN on the logits based on the mean and variance of all 1000 classes, we normalize using the statistics of the top 250 classes. The intuition of doing so is that the predicted probabilities of bottom classes

are extremely small and likely have negligible influence on model prediction and robustness. However, they considerably influence the mean and variance statistics of logits. Excluding these least-related classes makes the LN operation less noisy.

E.3. Relaxing the Independence Assumption in Theorem 4.4

Theorem 4.4 assumes that the margin of $h^M(X)$ and the correctness of $g(X)$ are independent. Suppose that such an assumption does not hold for a pair of base classifiers. Then, $\mathbb{P}_{X \sim \mathcal{X}_{ic}} [m_{h^M}(X) \geq \frac{1-\alpha}{\alpha}]$ may not be equal to $\mathbb{P}_{X \sim \mathcal{X}_{ic}} [m_{h^M}(X) \geq \frac{1-\alpha}{\alpha} \mid G_{\text{cor}}(X)]$. In this case, we need to minimize the latter quantity in order to effectively optimize (2). Hence, we need to modify the objective functions of (3) and (5) accordingly, and change the objective value assignment step in Line 10 of Algorithm 1 to $o^{ijk} \leftarrow \mathbb{P}_{X \in \tilde{\mathcal{X}}_{ic}} [m_{h^M_{\tilde{\mathcal{X}}_{ic}}}(X) \geq q_{1-\beta}^{ijk} \mid G_{\text{cor}}(X)]$. With such a modification, the optimization of s, p, c is no longer decoupled from $g(\cdot)$, but the resulting algorithm is still efficiently solvable and Theorem 4.4 still holds.

E.4. Approximation Quality of (6)

Algorithm 1 solves (6) as a surrogate of (5) for efficiency. One of the approximations of (6) is to use the minimum-margin perturbation against $h^{\text{LN}}(\cdot)$ instead of that associated with $h^M(\cdot)$. While $h^M(\cdot)$ and $h^{\text{LN}}(\cdot)$ are expected to have similar standalone accuracy and robustness, their confidence properties are different, and therefore the minimum-margin perturbation associated with $h^M(\cdot)$ can be different from that associated with $h^{\text{LN}}(\cdot)$, inducing a distribution mismatch. To analyze the influence of this mismatch on the effectiveness of Algorithm 1, we record the values of s^*, p^* , and c^* , compute the minimum-margin-AutoAttacked examples of $h^M_{\tilde{\mathcal{X}}_{ic}}(\cdot)$ and re-run Algorithm 1 with the new examples. If the objective value calculated via the new examples and s^*, p^*, c^* is close to the optimal objective returned from the original Algorithm 1, then the mismatch is small and benign and Algorithm 1 is capable of indirectly optimizing (5).

We use the CIFAR-100 model from Figure 1 as an example to perform this analysis. The original optimal objective returned by Algorithm 1 is 50.0%. The re-computed objective based on $h^M_{\tilde{\mathcal{X}}_{ic}}(\cdot)$'s minimum-margin perturbations, where $s^* = .612, p^* = 3.57, c^* = -2.14$, is 66.7%. While there is a gap between the two objective values and therefore the approximation-induced distribution mismatch exists, Algorithm 1 can still effectively decrease the objective value of (5).